RICE UNIVERSITY

Multiple Window Time-Frequency Analysis

by

Metin Bayram

A Thesis Submitted
in Partial Fulfillment of the
Requirements for the Degree

Master of Science

Approved, Thesis Committee:

Dr. Richard G. Baraniuk, Director
Assistant Professor of Electrical and
Computer Engineering

Dr. Don H. Johnson
Professor of Electrical and Computer
Engineering and of Statistics

Dr. Dennis Cox
Professor of Statistics

Houston, Texas

May, 1996

Multiple Window Time-Frequency Analysis

Metin Bayram

Abstract

The bias-variance trade-off is an important issue is spectrum estimation. In 1982, Thomson introduced a powerful multiple window method for stationary signals that deals with the bias-variance trade-off in an optimal fashion. In this thesis, we extend Thomson's method to the time-frequency and time-scale planes, and propose a new method to estimate the time-varying spectrum of non-stationary random processes. Unlike previous extensions of Thomson's method, we identify and utilize optimally concentrated window and wavelet functions, and develop a statistical test for detecting chirping line components. The optimal windows are the Hermite functions for time-frequency analysis, and the Morse wavelets for time-scale analysis.

Acknowledgments

During both the research and the preparation of this thesis, I was very fortunate to have the support and guidance of many people.

Starting with the academics, first of all I would like to thank my advisor Richard Baraniuk for his constant guidance and support. Through many hours of revisions of conference papers, he taught me the value of conciseness. Many thanks go to Dr. Don Johnson, who was a big influence on me to go to graduate school in the first place. He also kindly accepted to be on my thesis committee. I would also like to thank Dr. Dennis Cox for serving on my thesis committee. Several people have been very helpful to me and provided invaluable assistance during my research. Among these people, I would like to name Dr. Paulo Gonçalvès and Dr. Robert Nowak.

On the personal side, I thank my girlfriend Rebekah who was always there when I needed support. She has been great. A special thanks goes to my best friend Ediz for just being around. We will get a paper together some day. I cannot go without thanking my office mates Raghu and Andrew, and my other fellow EEs for providing a very friendly and productive environment in the department.

Finally, I would like to thank my parents and my brother Mert for all the support and encouragement they have given me for both my academic and non-academic life.

Contents

Abstract ii

Acknowledgments iii

List of Illustrations vi

1 Introduction 1

2 Time-Frequency Representations 4

2.1 Fourier Transform 4

2.2 Linear Time-Frequency Analysis 5

2.2.1 The Short-Time Fourier Transform 6

2.2.2 The Continuous Wavelet Transform 7

2.3 Bilinear Time-Frequency Analysis 9

2.3.1 Some Desirable Properties of Bilinear TFRs 10

2.3.2 Wigner Distribution 11

2.3.3 Cohen's Class 13

2.3.4 Affine Class 13

2.4 Time-Frequency Representations Of Random Processes 14

3 Multiple Window Time Varying Spectrum Estimation 17

3.1 Introduction 17

3.2 Thomson's Multiple Window Method 20

3.2.1 Summary of Thomson's Method 21

3.2.2 Prolate Spheroidal Functions 22
3.2.3 Thomson's F-test For Sinusoids 22
3.3 Multiple Window Time-Frequency Analysis 26
3.3.1 Hermite Windows 26
3.3.2 Multiple Window WVS Estimate 30
3.3.3 Cohen's Class Interpretation 30
3.3.4 Extraction Of Line Components 31
3.4 Multiple Window Time-Scale Analysis 38
3.4.1 Morse Wavelets 39
3.4.2 Multiple Window WVS Estimate 40
3.5 Examples 43

4 Discussion and Conclusions 45

Bibliography 47

Illustrations

1.1 *Three representations of the Gaussian-windowed linear chirp (1.1): (a) Real part of the signal. (b) Real part of the Fourier transform of the signal. (c) Wigner distribution of the signal.* 2

2.1 *(a) Real part of the test signal (2.1). (b) Real part of the Fourier transform of the test signal.* 5

2.2 *Idealized time-frequency representations of three STFT basis functions associated with different locations in the time-frequency plane.* 7

2.3 *Squared magnitude of the STFT of the test signal: (a) Long time window. (b) Short time window. (c) Medium time window.* 8

2.4 *Idealized time-frequency representations of three CWT basis functions associated with different locations in the time-frequency plane.* 9

2.5 *Squared magnitude of the CWT of the test signal.* 10

2.6 *The WD of the test signal.* 12

3.1 *(a) Test signal composed of a chirp with sinusoidal instantaneous frequency in an additive bandpass Gaussian noise of linearly rising center frequency. (b) Ideal representation. (c) Empirical Wigner distribution. (d) Spectrogram using a Gaussian window. (e) Sliding window Thomson's method as in [1–3]. (f) MW method.* 18

3.2 *The first three prolate windows in time.* 23

3.3 *True spectrum and three spectrum estimates of a stationary test signal composed of three sinusoids in a complex autoregressive process from [4]. The signal is discretized with 32 points and log scale is used for the plots. (a) True spectrum. (b) Hamming windowed periodogram. (c) Averaged periodogram with Hamming window (2 blocks of 16 points each). (d) Thomson's MW method using four windows.* 25

3.4 *(a) The circular concentration region (3.11) for the Hermite functions. (b) Eigenvalues of the localization operator over region (3.11) for different values of R* ($R_1 < R_2 < R_3$). 28

3.5 *From left to right the first three Hermite functions in the time domain, the frequency domain, and the time-frequency plane (WD): (a) 0-th order, (b) 1-st order (since the Fourier transform of the 1-st order Hermite function is purely imaginary, we plot the imaginary part), (c) 2-nd order.* 29

3.6 *(a) Test signal composed of a line component of sinusoidal instantaneous frequency. (b) Signal in additive white Gaussian noise 3.23.* 34

3.7 *Test statistic* $F(t, f)$ *before and after filtering for two different chirp rates for the test data in 3.23: (a) Corresponding to only spurious peaks. (b) Corresponding to true and spurious peaks.* 35

3.8 *Reassignment method: The value of the TFR computed at point* (t, f) *is assigned to the point* (t', f'). 38

3.9 *Smoothing regions in the time-frequency plane in (a) Cohen's class, (b) Affine class.* 39

3.10 *(a) The tear-drop shaped concentration region (3.27) for the Morse wavelets for* $\beta = \gamma = 1$ *equal to. (b) Eigenvalues of the localization operator for different values of* C $(C_1 < C_2 < C_3)$ *for* $\beta = \gamma = 1$. . . . 41

3.11 *From left to right the first three Morse wavelets in the time domain, the frequency domain (only the positive frequencies), and the time-frequency plane (WD): (a) 0-th order, (b) 1-st order, (c) 2-nd order.* 42

3.12 *Three spectrum estimates of the echo-location pulse emitted by the Large Brown Bat, Eptesicus Fuscus: (a) Empirical Wigner distribution. (b) Spectrogram. (c) Multiple window method.* 44

Chapter 1

Introduction

Spectrum estimation has been a field of interest for many years for both the engineering and the statistics communities. The theory of spectrum estimation is well developed for stationary signals — signals whose statistical properties do not change over time. For the non-stationary signals that we encounter in many applications, time-frequency representations prove to be essential, because they indicate how the power spectrum changes over time. To motivate the use of time-frequency representations, we present a simple example.

Consider a Gaussian-windowed linear chirp

$$s(t) = e^{-\alpha t^2} e^{j2\pi\left(f_0 t + c t^2\right)}, \qquad \alpha > 0\,, \tag{1.1}$$

with f_0 the frequency of the linear chirp at $t = 0$, and c the chirp rate. Figures 1.1(a) and 1.1(b) show this signal in time and frequency domains respectively. Figure 1.1(c) is the Wigner distribution of the signal. In the time and frequency representations of the signal in Figures 1.1(a) and 1.1(b), it is not obvious how different frequency components of the signal are distributed over time. The Wigner distribution of Figure 1.1(c) on the other hand shows clearly the time localization of frequency components.

This thesis is organized as follows: Chapter 2 gives a brief overview of time-frequency representations. Chapter 3 points out the limitations in time-varying spectrum estimation techniques, and proposes a method that is an extension of Thomson's

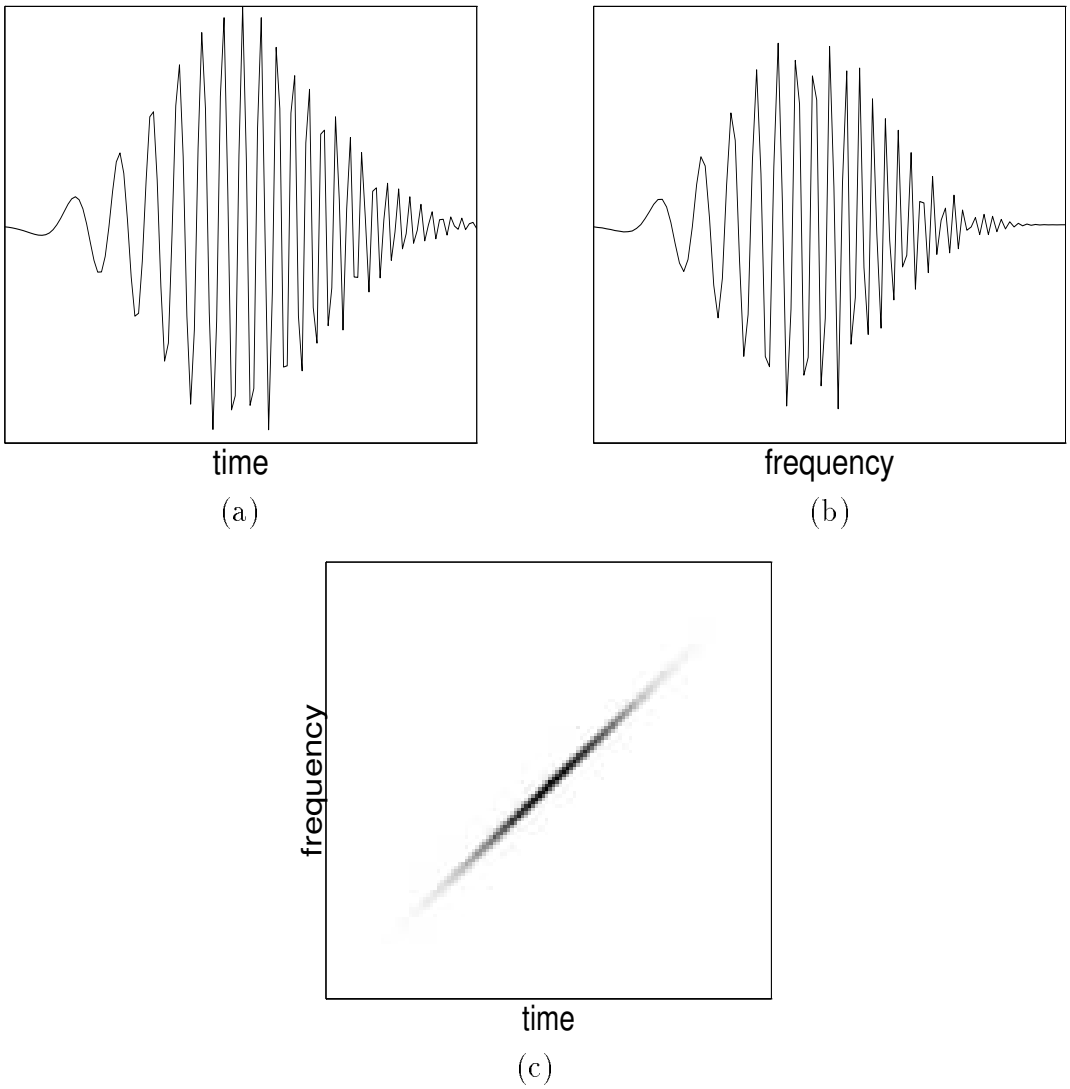

Figure 1.1: *Three representations of the Gaussian-windowed linear chirp (1.1): (a) Real part of the signal. (b) Real part of the Fourier transform of the signal. (c) Wigner distribution of the signal.*

multiple-window method for stationary signals to the time-frequency and time-scale planes. We discuss the contributions and conclusions in Chapter 4.

Chapter 2

Time-Frequency Representations

In this chapter, we give a brief overview of time-frequency representations (TFR). For more details, the interested reader should consult the excellent books by Cohen [5], Priestley [6] and Daubechies [7], and the papers by Cohen [8], Martin and Flandrin [9], Rioul and Vetterli [10], Hlawatsch and Boudreaux-Bartels [11], and Rioul and Flandrin [12].

Consider the following multicomponent test signal

$$s(t) = e^{-\alpha(t-t_1)^2} e^{j2\pi f_1 t} + e^{-\alpha(t-t_2)^2} e^{j2\pi f_2 t}, \qquad \alpha > 0 \tag{2.1}$$

composed of two Gaussian bumps centered at (t_1, f_1) and (t_2, f_2) respectively. We show the signal and its Fourier transform in Figure 2.1. For the discussion that follows, all TFRs will be demonstrated using this test signal.

2.1 Fourier Transform

The Fourier transform $X(f)$ of a signal $x(t)$ is defined as

$$X(f) = \int_{-\infty}^{\infty} x(t) e^{-j2\pi f t} dt. \tag{2.2}$$

The signal $x(t)$ can be recovered from $X(f)$ through the inverse Fourier transform

$$x(t) = \int_{-\infty}^{\infty} X(f) e^{j2\pi f t} df. \tag{2.3}$$

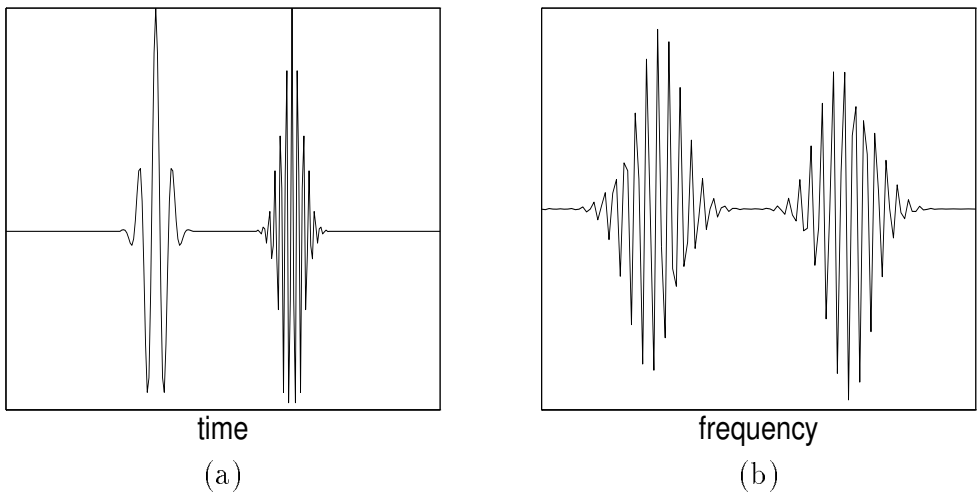

Figure 2.1: *(a) Real part of the test signal (2.1). (b) Real part of the Fourier transform of the test signal.*

The Fourier transform of a signal gives information about the frequency content of the signal. However, it does not give any explicit indication about when a certain frequency component is present (actually, this information is hidden in the phase), because the value of the Fourier transform at frequency f is computed by averaging the contributions from all time. This restriction of the Fourier transform led to the introduction of time-frequency representations (TFR). TFRs are two-dimensional transformations that indicate the joint time-frequency content of signals.

2.2 Linear Time-Frequency Analysis

These TFRs satisfy the superposition principle which states that if $x(t)$ is a linear combination of $x_1(t)$ and $x_2(t)$ then, the TFR of $x(t)$ is the same linear combination of the TFRs of $x_1(t)$ and $x_2(t)$

$$x(t) = c_1 x_1(t) + c_2 x_2(t) \quad \Rightarrow \quad TFR_x(t,f) = c_1\, TFR_{x_1}(t,f) + c_2 TFR_{x_2}(t,f) \qquad (2.4)$$

where TFR_x is the TFR of x.

Two important linear TFRs are the short-time Fourier transform (STFT) and the continuous wavelet transform (CWT).

2.2.1 The Short-Time Fourier Transform

STFT localizes frequency components in time by sliding a window $h(t)$ along the signal $x(t)$ and taking the Fourier transform [5, 8, 11]

$$STFT_x(t,f) = \int_{-\infty}^{\infty} x(\tau)h(\tau - t)e^{-j2\pi f\tau}d\tau. \tag{2.5}$$

The above representation can also be expressed as the projection of the signal on the basis functions

$$\left\{h(\tau - t)e^{-j2\pi f\tau}\right\}_{(t,f)\in\mathbb{R}^2}. \tag{2.6}$$

Since these basis functions are translated and modulated versions of the window $h(t)$, they are centered at different locations in the time-frequency plane. Figure 2.2 shows the idealized time-frequency representations of the STFT basis functions associated with three different locations in the time-frequency plane. Note that the shape of these representations are the same for all three of them illustrating the fixed time-frequency resolution of the STFT once a window is chosen. Good time resolution is achieved by a short window, whereas good frequency resolution is achieved by a long window. The fact that the time and frequency resolutions cannot be made better simultaneously is known as *Heisenberg uncertainty principle*. In Figure 2.3, we show the squared magnitude of the STFT (spectrogram) of the test signal corresponding to long, short, and medium time windows. Again, the fixed time-frequency resolution is evident.

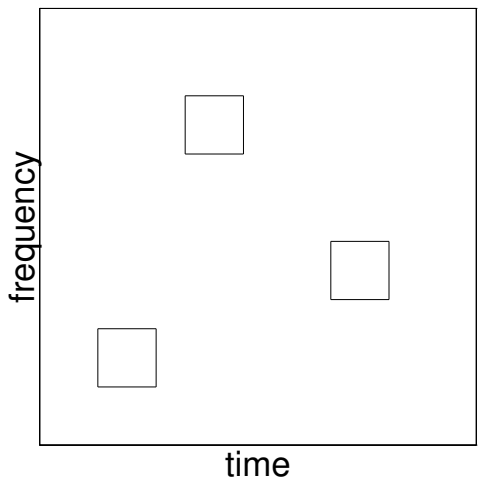

Figure 2.2: *Idealized time-frequency representations of three STFT basis functions associated with different locations in the time-frequency plane.*

2.2.2 The Continuous Wavelet Transform

The CWT of signal $x(t)$ is defined as [10]

$$CWT_x(t,a) = a^{-1/2} \int_{-\infty}^{\infty} x(\tau)\, \psi^*\left(\frac{\tau - t}{a}\right)\, d\tau \tag{2.7}$$

where $\psi(t)$, called the analyzing wavelet, is a bandpass function centered around $t = 0$, and a is the scale. Scale can be interpreted in terms of frequency f as $a = \frac{f_0}{f}$ where f_0 is the center frequency of the Fourier transform of $\psi(t)$.

Similarly to the STFT, the CWT can be expressed as the projection of the signal on the basis functions

$$\left\{ \sqrt{\frac{f}{f_0}}\ \psi\left(\frac{f}{f_0}(\tau - t)\right) \right\}_{(t,f)\in\mathbb{R}^2}. \tag{2.8}$$

These basis functions change their shape with frequency. Therefore, unlike the STFT, the time-frequency resolution of the CWT is frequency dependent. To analyze low frequency components the analyzing wavelet is dilated in time and compressed in

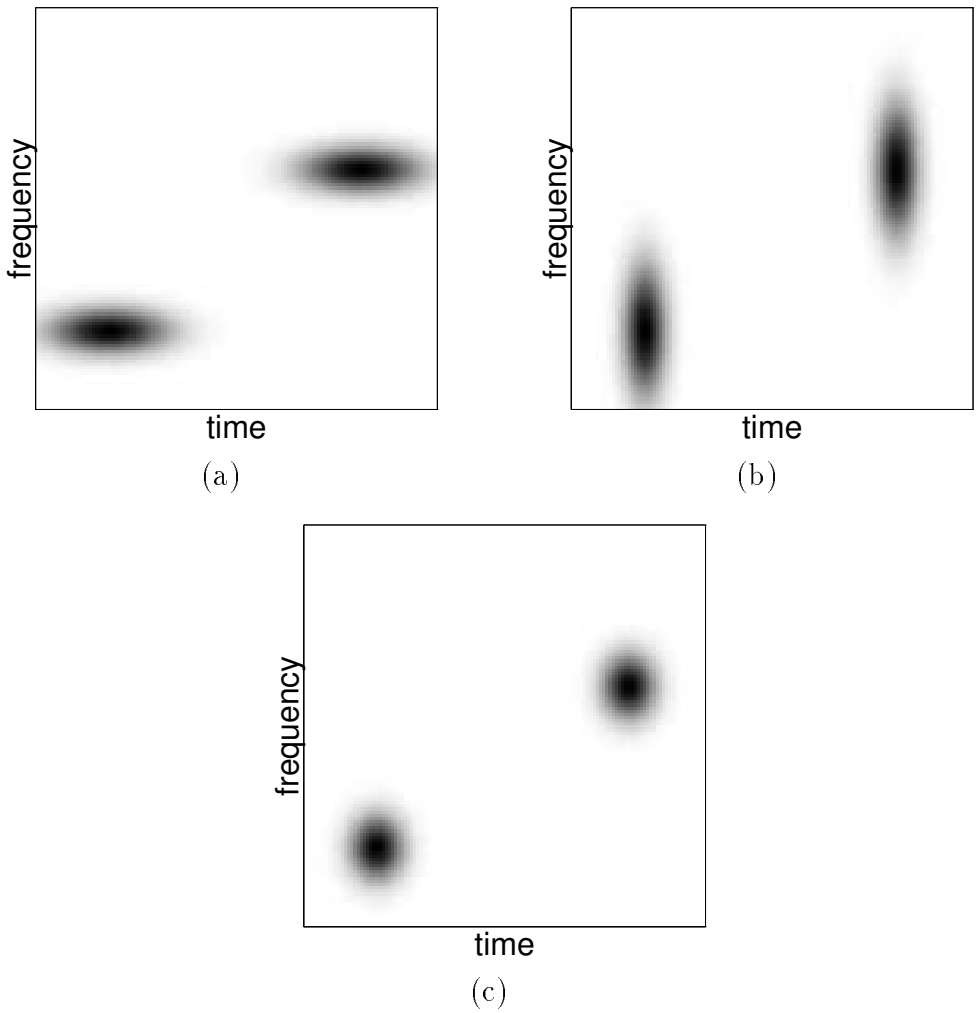

Figure 2.3: *Squared magnitude of the STFT of the test signal: (a) Long time window. (b) Short time window. (c) Medium time window.*

frequency, whereas to analyze high frequency components the analyzing wavelet is dilated in frequency and compressed in time. This property of the CWT makes it very suitable for signals with high frequency content of short duration and low frequency content of long duration. Figure 2.4 shows the idealized time-frequency representations of the CWT basis functions associated with three different locations of the time-frequency plane. Note that the shape changes with frequency illustrating the frequency dependent time-frequency resolution of the CWT. In Figure 2.5 we show the squared magnitude of the CWT (scalogram) of the test signal.

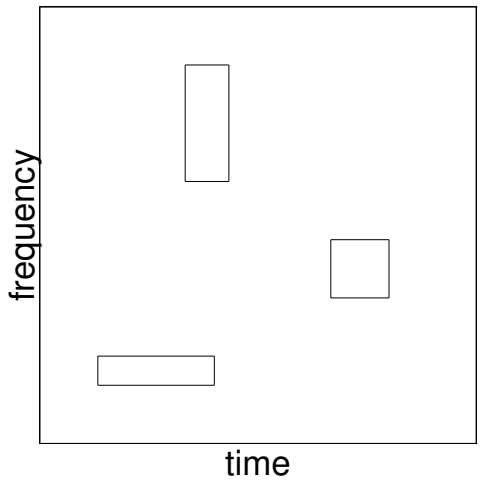

Figure 2.4: *Idealized time-frequency representations of three CWT basis functions associated with different locations in the time-frequency plane.*

2.3 Bilinear Time-Frequency Analysis

Although linearity of a TFR is a desirable property, bilinear TFRs are intuitive if we want to interpret them as time-frequency energy distributions since energy is a quadratic function of the signal. A bilinear TFR $TFR_x(t, f)$ of signal x seeks to combine the instantaneous power $|x(t)|^2$ and the spectral energy density $|X(f)|^2$ into

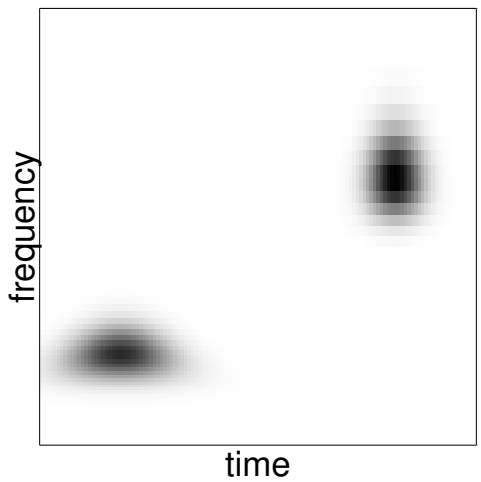

Figure 2.5: *Squared magnitude of the CWT of the test signal.*

one representation. For example, squaring the STFT and the CWT gives two bilinear TFRs — the spectrogram and the scalogram respectively.

2.3.1 Some Desirable Properties of Bilinear TFRs

1. Marginals:

$$\int_{-\infty}^{\infty} TFR_x(t,f)\,df = |x(t)|^2\,, \tag{2.9}$$

$$\int_{-\infty}^{\infty} TFR_x(t,f)\,dt = |X(f)|^2\,. \tag{2.10}$$

2. Real-valued and positive so that they can be interpreted as energy distributions.

3. Conservation of time and frequency shifts:

$$\begin{array}{ccc} x(t) & \longrightarrow & x(t-t_0)\,e^{j2\pi f_0 t} \\ \downarrow & & \downarrow \\ TFR_x(t,f) & \longrightarrow & TFR_x(t-t_0, f-f_0) \end{array} \tag{2.11}$$

4. Conservation of time-frequency scaling:

$$\begin{array}{ccc} x(t) & \longrightarrow & \sqrt{|a|}\,x(at) \\ \downarrow & & \downarrow \\ TFR_x(t,f) & & TFR_x\left(at, \frac{f}{a}\right) \end{array} \tag{2.12}$$

5. Unitarity (Moyal's formula)

$$\int_{-\infty}^{\infty}\int_{-\infty}^{\infty} TFR_x(t,f)\, TFR_y(t,f)\, dt\, df = \left| \int_{-\infty}^{\infty} x(t)\, y^*(t)\, dt\, df \right|^2. \tag{2.13}$$

Although it is impossible to meet all the desirable properties for the TFRs [5,8,11], the Wigner distribution is one that satisfies a large number of properties. We next introduce this important TFR on which most of time-frequency analysis builds.

2.3.2 Wigner Distribution

The Wigner distribution (WD) of signal x is defined as [5]

$$W_x(t,f) = \int_{-\infty}^{\infty} x\left(t + \frac{\tau}{2}\right) x^*\left(t - \frac{\tau}{2}\right) e^{-j2\pi f\tau} d\tau. \tag{2.14}$$

The WD can be interpreted as a STFT where the window is matched to the signal (the window is the time reversed signal). This property makes the concentration of the WD the best among all TFRs.

The WD satisfies a large number of desired mathematical properties. It satisfies the marginal properties (2.9) and (2.10), it is real-valued, it is covariant to time-frequency shifts and time-frequency scaling, and it is a unitary transformation. Although all these properties make the WD very desirable, it suffers from two major drawbacks: 1) It can take on negative values that prevents it from being strictly interpreted as an energy distribution. 2) Because of its bilinear nature, it produces artifacts called *cross-components* [5,8,11].

Cross-Components

The WD of the sum of two signals x and y is given by

$$W_{x+y}(t,f) = W_x(t,f) + W_y(t,f) + 2\,\mathrm{Re}\left[W_{x,y}(t,f)\right]. \tag{2.15}$$

The first two terms on the right hand side of (2.15) correspond to x and y respectively, and are called the *auto-components*. The last term is the *cross-component* between x and y, given by

$$W_{x,y}(t,f) = \int_{-\infty}^{\infty} x\left(t+\frac{\tau}{2}\right) y^*\left(t-\frac{\tau}{2}\right) e^{-j2\pi f\tau} d\tau. \tag{2.16}$$

It is an artifact produced as a result of the quadratic nature of the WD. Figure 2.6 shows the WD of the test signal. The cross-component can be seen centered between the two auto-components.

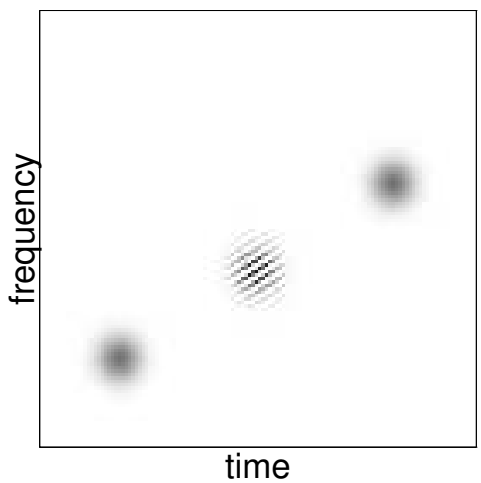

Figure 2.6: *The WD of the test signal.*

The number of cross-components in the WD increases with the number of components in the signal. An n-component signal has $\frac{n(n-1)}{2}$ cross components [5, 8, 11].

For multicomponent or noisy signals, these cross-components make the WD very difficult to interpret. It becomes necessary to suppress the cross-components to obtain readable TFRs.

2.3.3 Cohen's Class

The oscillatory cross-components of the WD can be suppressed by convolving the WD with a kernel in the time-frequency plane to obtain a new bilinear TFR

$$C_x(t,f) = W_x(t,f) \; ** \; \Phi(t,f). \tag{2.17}$$

The class of all TFRs obtained from the WD via convolution with a kernel is known as Cohen's class [5, 8, 11]. The TFRs in this class satisfy the time-frequency shift covariance property (2.11).

Some TFRs in Cohen's class are the spectrogram which is the squared magnitude of the STFT, the WD itself, and the Choi-Williams distribution [13].[1] These TFRs and their kernels are given in Table 2.1.

2.3.4 Affine Class

The class of all time-scale representations (TSR) that are covariant to time shifts and scale changes is called the affine class. Distributions in this class satisfy the time-frequency scaling property (2.12) and can be written as

$$TSR_x(t,a) = \int_{-\infty}^{\infty} \int_{-\infty}^{\infty} W_x(\tau,\nu)\, \Pi\left(\frac{\tau - t}{a}, a\nu\right) d\tau d\nu \tag{2.18}$$

where Π is the kernel that characterizes the distribution and W_x is the WD of x [12].

[1] [5] has a list of all TFRs in Cohen's class and their kernels.

Table 2.1: *Some TFRs in Cohen's Class and Their Kernels.*

TFR	Kernel
Spectrogram	$W_h(t,f)$
Wigner	$\delta(t)\,\delta(f)$
Choi-Williams	$\iint e^{-\frac{\theta^2\tau^2}{\sigma}}\, e^{j2\pi t\theta}\, e^{-j2\pi f\sigma}\, d\theta\, d\sigma$

The scalogram which is the squared magnitude of the CWT is a distribution in the affine class. Its kernel is the WD of the analyzing wavelet. The Wigner and the Choi-Williams distributions are in the affine class as well as in the Cohen's class of TFRs.

2.4 Time-Frequency Representations Of Random Processes

Time-frequency analysis is not limited just to deterministic signals. In this section, we look at two extensions of the stationary power spectrum to the time-frequency plane.

The power spectrum of a stationary random process is defined as the Fourier transform of the autocorrelation function of the process

$$P_x(f) = \int_{-\infty}^{\infty} r_x(\tau)\, e^{-j2\pi f\tau}\, d\tau \tag{2.19}$$

where

$$r_x(\tau) = E[x(t)\, x^*(t+\tau)] \tag{2.20}$$

is the autocorrelation function of $x(t)$. The problem of stationary power spectrum estimation is then to estimate $P_x(f)$ given only part of one realization of the stationary process $x(t)$. This problem has been well studied over the past decades [4].

Unlike the power spectrum for stationary random processes, there is no unique definition for the time-varying spectrum of a non-stationary random process (This is due to the fact that there is no TFR that satisfies all the requirements of an energy density).

A number of definitions have been proposed for the time-varying spectrum of non-stationary processes [6, 9]. None of these are completely satisfactory because it is impossible to meet all requirements of a true time-varying spectrum. We would like to mention two notable definitions here. The *evolutionary spectrum* proposed by Priestley is defined for a certain class of non-stationary processes called oscillatory processes [6]. It is not unique and it does not have an interpretation in terms of the correlation function. For these two reasons, we do not use it as our definition for the non-stationary spectrum. In this thesis, we choose the *Wigner-Ville spectrum* (WVS) proposed by Martin and Flandrin [9] as our definition of the time-varying spectrum. The WVS $\mathbf{W}_x$ is defined as the Fourier transform of the autocorrelation function $r_x(t,\tau)$ of the non-stationary process $x(t)$

$$\mathbf{W}_x(t,f) = \int_{-\infty}^{\infty} r_x(t,\tau)\, e^{-j2\pi f\tau}\, d\tau \tag{2.21}$$

where

$$r_x(t,\tau) = E\left[x\left(t+\frac{\tau}{2}\right)\, x^*\left(t-\frac{\tau}{2}\right)\right]. \tag{2.22}$$

Below are some of the attractive properties of the WVS that make it a popular choice for the time-varying spectrum:

1. The WVS can be written as the expected value of the Wigner distribution W_x of one realization of the process $x(t)$

$$\mathbf{W}_x(t,f) = E[W_x(t,f)]. \tag{2.23}$$

2. The WVS is unique for a given process.

3. The WVS reduces to the usual power spectrum density for stationary signals. This can be seen from (2.22) since $r_x(t,\tau) = r_x(\tau)$ for a stationary process.

In the next chapter we begin with a discussion of several methods used to estimate the WVS given only part of one realization of a non-stationary process. We discuss some of the limitations of these methods, and propose a new method that extends Thomson's powerful multiple window method for stationary signals to the WVS estimation of non-stationary processes.

Chapter 3

Multiple Window Time Varying Spectrum Estimation

3.1 Introduction

Many methods exist for estimating the power spectrum of stationary signals [4]. However, these methods are insufficient for the non-stationary signals that occur in important applications such as radar, sonar, acoustics, biology, and geophysics. These applications demand time-frequency representations that indicate how the power spectrum changes over time. To date research in time-frequency analysis has focused on deterministic signals. Only recently has attention turned to non-stationary random processes [1–3, 9, 14].

As we mentioned in Chapter 2, we choose the *Wigner-Ville spectrum* (WVS) [9] as our definition of the time-varying spectrum in this thesis. Figure 3.1 shows a test signal composed of a chirp with sinusoidal instantaneous frequency in an additive bandpass Gaussian noise of linearly rising center frequency, and its ideal time-varying spectrum together with four different estimates of the WVS of the test signal.

A number of different WVS estimates have been proposed. The simplest is the empirical Wigner distribution $W_x(t, f)$ (WD) itself. However, while it is unbiased, it has very large (infinite in theory) variance and cross-components as mentioned in

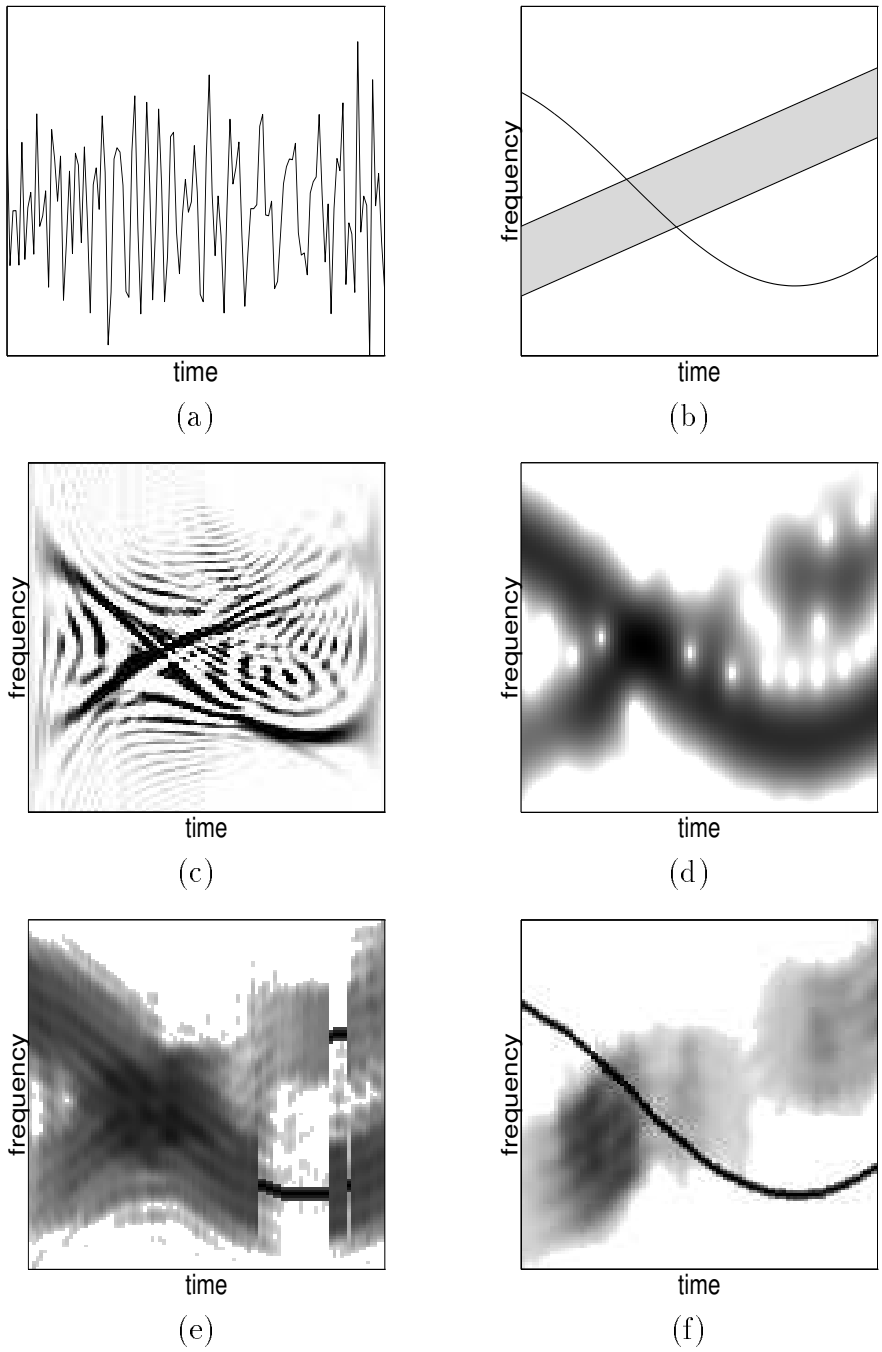

Figure 3.1: *(a) Test signal composed of a chirp with sinusoidal instantaneous frequency in an additive bandpass Gaussian noise of linearly rising center frequency. (b) Ideal representation. (c) Empirical Wigner distribution. (d) Spectrogram using a Gaussian window. (e) Sliding window Thomson's method as in [1–3]. (f) MW method.*

Section 2.3.2. The large variance and the cross components of the empirical WD make it very difficult to interpret the WVS estimate, as can be seen in Figure 3.1(c).

To overcome the large variance problem of the WD, two-dimensional convolution of the Wigner distribution with a signal-independent smoothing kernel can be performed [9]. Sayeed and Jones [14] have developed a method for optimal kernel design for WVS estimation when the statistics of the process are known. They minimize the mean-squared error between the true WVS and the estimate, and also address the problem of local WVS estimation by allowing the smoothing kernel to be signal dependent. Whether the kernels are signal independent or signal dependent, the large amount of smoothing required to obtain a low variance WVS estimate can damage the resolution of line components in the data. Line components are deterministic chirping signals of the form $e^{j2\pi\gamma(t)}$, whose ideal time-frequency representations have the form $\delta(f-\gamma'(t))$. Figure 3.1(d) shows the effect of smoothing on the line components using the spectrogram with a Gaussian window.

Realizing that random and deterministic spectral components must be dealt with separately, Thomson introduced a powerful multiple window (MW) spectrum estimator for stationary signals in [15] to obtain a low variance spectrum without degrading the resolution of line components. The method uses a statistical significance test to detect and extract all sinusoids (the only stationary deterministic line components) from the data, computes a MW spectrum estimate of the sinusoid-free data with optimal windows, and reshapes the spectrum to account for the excised sinusoids. Because of its excellent performance, several groups have applied this technique, ad hoc, to non-stationary signals in a piecewise fashion [1–3,16]. There are two problems in doing this: 1) The windows used by Thomson are not optimal in a time-frequency setting, 2) The chirping rate of the line components must be very small so that they

can be approximated as piece-wise sinusoids. Figure 3.1(e) shows the sliding window Thomson's method applied to the test signal. It can be seen that the method comes short of detecting the line component.

In this thesis we refine the previous extensions of Thomson's method into an improved time-varying MW spectrum estimate for non-stationary signals by: 1) identifying the optimal windows to use, and 2) developing a statistical test to detect line components of the form $e^{j2\pi\gamma(t)}$. Our method preserves the resolution of line components, has low variance, and offers fine control over the bias-variance trade-off. Figure 3.1(f) shows our method applied to the test signal.

This chapter is organized as follows. In Section 3.2 we give a brief review of Thomson's MW method for stationary signals, and explain the essence of his significance test for sinusoids. Section 3.3 discusses MW time-frequency analysis. We identify the optimal windows to use in the MW method, and extend the significance test to include all line components of the form $e^{j2\pi\gamma(t)}$. In Section 3.4, we extend the ideas in Section 3.3 to the time-scale plane, again identifying the optimal windows. Finally, Section 3.5 demonstrates the performance of our method. We begin with a review of Thomson's MW method for stationary signals.

3.2 Thomson's Multiple Window Method

The classical spectrum estimator for stationary signals, the periodogram, is defined as simply the squared magnitude of the Fourier transform of the windowed data

$$\widehat{P}_x(f) = \left| \int x(t)\, w(t)\, e^{-j2\pi f t}\, dt \right|^2 \tag{3.1}$$

where $w(t)$ is the window function. While the periodogram suffers from large variance, this variance can be reduced by cutting the data into blocks, computing a periodogram

of each block, and then averaging the periodograms [4]. However, this procedure also smoothes and biases the resulting spectrum estimate. The increase in bias is due to using a shorter window for each block.

Inspired by the notion of averaging but displeased with the resulting bias, Thomson suggested computing several periodogram estimates of the *entire signal* using a set of different windows and then averaging the resulting periodograms to construct a spectrum estimate [15]. For a low variance, low bias estimate, he demanded that the windows be 1) orthogonal (to minimize variance), and 2) optimally concentrated in frequency (to minimize bias). The optimal windows satisfying these requirements for signals of finite extent are the prolate spheroidal functions. In addition to multiple windows, Thomson also introduced into his estimate a separate procedure for deterministic sinusoidal components as mentioned above.

3.2.1 Summary of Thomson's Method

Thomson's MW method can be summarized in three steps [15]:

1. Detect and extract all significant sinusoids (stationary deterministic line components) in the data $x(t)$ using a statistical significance test (see Section 3.2.3) to obtain the part $y(t)$ of the data having a continuous spectrum[2]

$$y(t) = x(t) - \{sinusoids\}. \tag{3.2}$$

2. Average K "orthogonal" periodogram estimates of $y(t)$ using prolate spheroidal data windows $\{v_k(t)\}$ (see Section 3.2.2) [17]

$$P_T(f) = \frac{1}{K} \sum_{k=0}^{K-1} \frac{1}{\lambda_k} \left| \int y(t)\, v_k(t)\, e^{-j2\pi f t}\, dt \right|^2 . \tag{3.3}$$

[2]In [15], Thomson sets up the spectrum estimation problem in discrete-time.

where λ_k is the eigenvalue of the operator in Section 3.2.2 corresponding to the k-th order prolate function. In the above estimate the first K prolate windows are used for which the eigenvalues are very close to one. This guarantees a minimized introduced bias due to the averaging [15].

3. Reshape the spectrum $P_T(f)$ to account for the sinusoids excised in Step 1.

3.2.2 Prolate Spheroidal Functions

The prolate spheroidal functions are the eigenfunctions of the operator $\mathcal{Q}_T\mathcal{P}_\Omega\mathcal{Q}_T$ where $\mathcal{Q}_T$ is the time-limiting operator

$$(\mathcal{Q}_T g)(t) = \begin{cases} g(t) & \text{if } |t| \leq T \\ 0 & \text{otherwise} \end{cases} \tag{3.4}$$

and $\mathcal{P}_\Omega$ is the band-limiting operator

$$\mathcal{F}(\mathcal{P}_\Omega g)(f) = \begin{cases} G(f) & \text{if } |f| \leq \Omega \\ 0 & \text{otherwise} \end{cases} \tag{3.5}$$

where $\mathcal{F}$ denotes the Fourier transform operation, and G is the Fourier transform of g.

These functions are perfectly suited to stationary spectrum estimation, because they are simultaneously compactly supported in time and optimally concentrated in frequency [17]. This concentration property results in a low bias estimate of the spectrum. The first three prolate functions are shown in Figure 3.2.

3.2.3 Thomson's F-test For Sinusoids

Before we can extract the significant sinusoids from the data $x(t)$ as in (3.2), we must detect their presence and estimate their parameters.

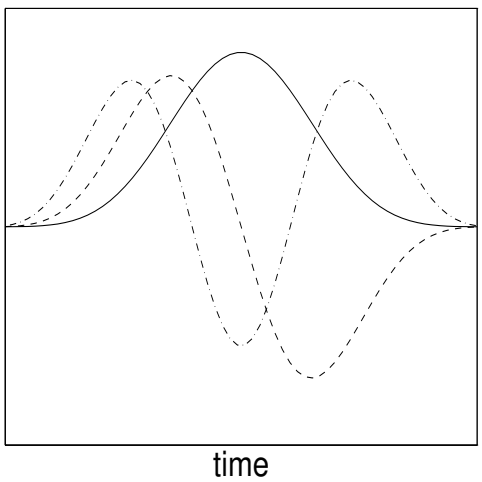

Figure 3.2: *The first three prolate windows in time.*

We assume the signal model

$$x(t) = y(t) + \sum_i \mu(f_i)\, e^{j2\pi f_i t} \tag{3.6}$$

with $y(t)$ zero mean and Gaussian. Define the k-th eigenspectrum $\chi_k(f)$ as the Fourier transform of the windowed data

$$\chi_k(f) = \int x(t)\, v_k(t)\, e^{-j2\pi f t}\, dt. \tag{3.7}$$

The expected value of $\chi_k(f)$ at f_i is given by

$$E[\chi_k(f_i)] = \mu(f_i)\, V_k(0) \tag{3.8}$$

where $V_k(f)$ is the Fourier transform of $v_k(t)$. Thus, using a simple linear regression, the complex amplitude $\mu(f_i)$ of each possible sinusoid can be estimated as

$$\widehat{\mu}(f_i) = \frac{\sum_{k=0}^{K-1} V_k(0)\, \chi_k(f_i)}{\sum_{k=0}^{K-1} V_k^2(0)}. \tag{3.9}$$

where K is the number of windows used for the estimation.

The eigenspectra yield a simple statistical test for whether sinusoids are really present in the data. Assuming that a sinusoid is present at frequency f, we subtract it from the data to obtain an estimate of the "background" continuous spectrum around f. Comparing this power in the background spectrum with the power in the assumed sinusoid results in an F variance-ratio test [15] with 2 and $2K-2$ degrees of freedom for the significance of the estimated line component

$$F(f) = \frac{(K-1)\,\widehat{\mu}(f)^2 \sum_{k=0}^{K-1} V_k(0)^2}{\sum_{k=0}^{K-1} \left|\chi_k(f) - \widehat{\mu}(f)\,V_k(0)\right|^2}. \tag{3.10}$$

If $F(f)$ exceeds a significance threshold, we say that a sinusoid exists at frequency f.

The probability of a miss increases with the threshold. A miss occurs when the method cannot detect an existing sinusoid. On the other hand, the false alarm probability increases with decreasing threshold. A false alarm or a *spurious peak* occurs when the method detects a non-existing sinusoid.

Figure 3.3 demonstrates the superior performance of Thomson's MW method applied to a stationary test data set that is composed of three sinusoids in a complex autoregressive process. Only 32 data points are available. Figure 3.3(a) is the true spectrum.

Averaging orthogonal periodogram estimates reduces the variance of the MW power spectrum estimate by approximately K times compared to the variance of a single periodogram (in which $K = 1$). Furthermore, concentrated windows and sinusoid extraction keep resolution very high. These properties make Thomson's MW method the tool of choice for estimating the power spectrum of stationary random processes.

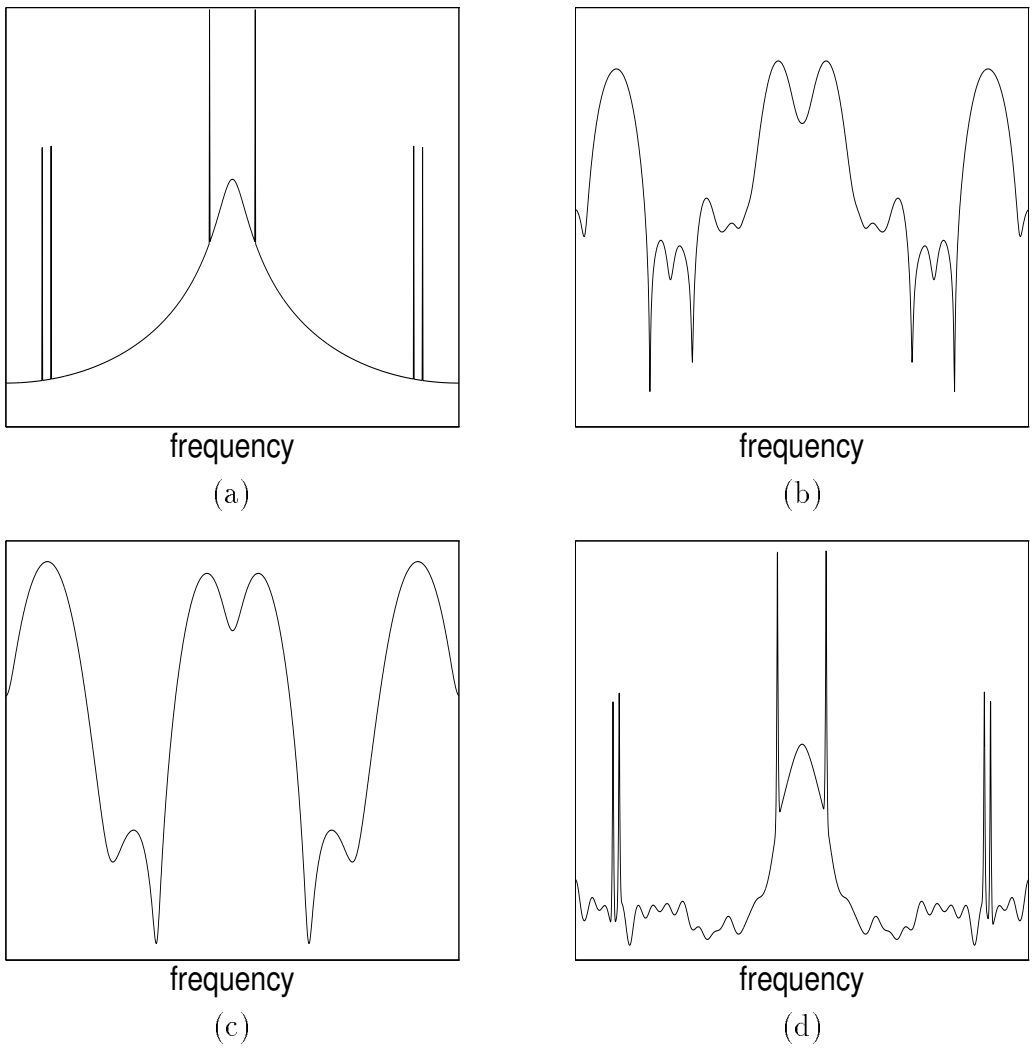

Figure 3.3: *True spectrum and three spectrum estimates of a stationary test signal composed of three sinusoids in a complex autoregressive process from [4]. The signal is discretized with 32 points and log scale is used for the plots. (a) True spectrum. (b) Hamming windowed periodogram. (c) Averaged periodogram with Hamming window (2 blocks of 16 points each). (d) Thomson's MW method using four windows.*

3.3 Multiple Window Time-Frequency Analysis

The excellent performance of Thomson's MW method has led several groups to apply the method to time-varying spectrum estimation by simply sliding the estimate (3.3) along the signal and computing a MW spectrogram estimate about each time point [1–3, 16]. While reasonably effective on certain classes of piecewise stationary signals, this approach suffers from two primary drawbacks. First, prolate spheroidal window functions have no inherent optimality properties in the joint time-frequency domain. Second, Thomson's F-test sinusoid extraction procedure fails on chirping line components of rapidly changing instantaneous frequency as we saw in Figure 3.1(e). In this section, we will extend Thomson's MW method to the time-frequency and time-scale planes by identifying sets of optimal windows/wavelets, and by developing a linear-chirp extraction algorithm that better matches non-stationary line components.

3.3.1 Hermite Windows

The foundation of the stationary MW method rests on the fact that the prolate spheroidal functions are optimal windows for estimating the spectrum of a time-limited signal. This optimality does not carry over into time-frequency, however, since the prolate spheroidal functions treat the time-frequency plane as two separate spaces rather than as one geometric whole [18–20].

For time-frequency signal analysis, it is natural to average over multiple orthogonal windows that are optimally concentrated in an appropriate time-frequency domain. To date, optimal orthogonal functions of this kind have been found only for a few very special domains. For instance, the Hermite functions are optimally concentrated

in the circular time-frequency region of Figure 3.4(a)

$$\left\{(t,f): \quad t^2+f^2 \leq R^2\right\} \tag{3.11}$$

with R a constant, and thus treat all time-varying spectral features in the same fashion [18–20]. The Hermite functions are the eigenfunctions of a localization operator over region (3.11) [18]. This operator localizes functions in joint time-frequency as opposed to the localization operator for the prolate functions that localizes functions in time and frequency separately. The k-th order Hermite function is defined as

$$h_k(t) = \pi^{-1/4}(2^k k!)^{-1/2} p_k(t) e^{-\frac{t^2}{2}}, \qquad k = 0, 1, 2, \cdots \tag{3.12}$$

where

$$p_k(t) = (-1)^k e^{t^2} \left(\frac{d}{dt}\right)^k e^{-t^2} \tag{3.13}$$

is the k-th order Hermite polynomial. The eigenvalues of the the localization operator over the region (3.11) are given by

$$\lambda_k(R) = 1 - e^{\frac{-R^2}{2}} \sum_{i=0}^{k} \frac{1}{i!} 2^{-i} R^{2i}. \tag{3.14}$$

In Figure 3.4(b) we show the behavior of these eigenfunctions. Since these are the eigenfunctions of a localization operator, the closer the k-th eigenvalue is to one the better the concentration of the k-th order Hermite function. Hence, for a given R, there are only a few Hermite functions with good concentration in region (3.11). Some properties of the Hermite functions are:

1. The Hermite polynomials and hence the Hermite functions can easily be computed through the recursion formula

$$p_{k+1}(t) = 2tp_k(t) - 2kp_{k-1}(t) \tag{3.15}$$

with $p_0(t) = 1$, and $p_1(t) = 2t$.

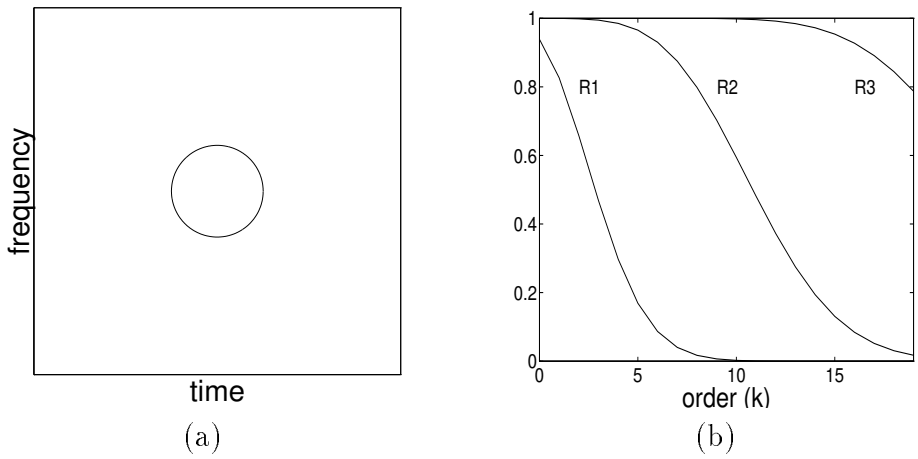

Figure 3.4: *(a) The circular concentration region (3.11) for the Hermite functions. (b) Eigenvalues of the localization operator over region (3.11) for different values of R ($R_1 < R_2 < R_3$).*

2. The k-th order Hermite polynomial $p_k(t)$ is an even function of t if k is even, and an odd function of t if k is odd.

3. The Hermite functions h_k are the eigenfunctions of the Fourier transform

$$(\mathcal{F}h_k(t)) = (2\pi)^{1/2}(-j)^k h_k(f) \tag{3.16}$$

   where $\mathcal{F}$ denotes the Fourier transform operation.

4. The Hermite functions h_k form an orthonormal basis for $L^2(\mathbb{R})$, the Hilbert space of square integrable functions.

Figure 3.5 shows the first three Hermite functions in time, their Fourier transforms, and their Wigner distributions. Comparing this figure with Figure 3.4(a), we see how the shape of the Wigner distribution of each Hermite function matches the shape of the concentration region. Hermite functions concentrated in elliptical regions are easily obtained by compressing or dilating the above functions $h_k(t)$.

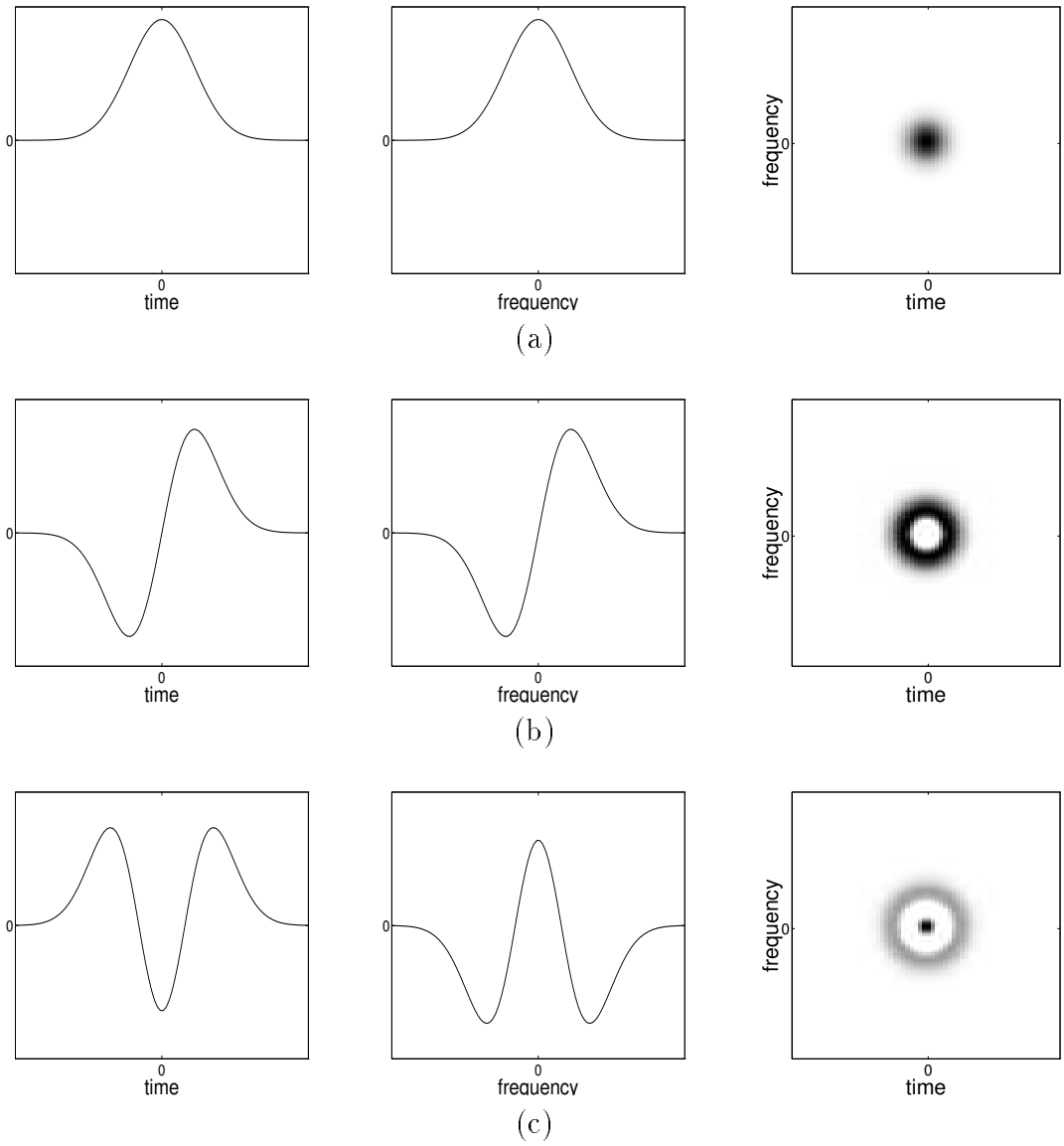

Figure 3.5: *From left to right the first three Hermite functions in the time domain, the frequency domain, and the time-frequency plane (WD): (a) 0-th order, (b) 1-st order (since the Fourier transform of the 1-st order Hermite function is purely imaginary, we plot the imaginary part), (c) 2-nd order.*

3.3.2 Multiple Window WVS Estimate

Thomson's MW spectrum average (3.3) estimates the energy content of the signal at frequency f by projecting onto the windowed sinusoids $v_k(t)\, e^{j2\pi f t}$. By analogy, we estimate the energy content of a non-stationary signal at time t and frequency f by projecting onto the sliding windowed sinusoids $h_k(\tau - t)\, e^{j2\pi f \tau}$. The result can be written as the average of K Hermite-windowed spectrograms of the data

$$\widehat{\mathbf{W}}_x(t,f) = \frac{1}{K} \sum_{k=0}^{K-1} \left| \int y(\tau)\, h_k(\tau - t)\, e^{-j2\pi f \tau} d\tau \right|^2. \tag{3.17}$$

The value of K is such that for a chosen R in (3.11) the first K eigenvalues in (3.14) are very close to one. The smaller the value of R, the smaller the bias of the estimate, and the smaller the value of K. Therefore, we see the bias-variance trade-off reflecting in the choice of K and R. The WVS estimator has low variance thanks to the averaging but also minimized bias due to the optimal concentration of the Hermite windows. The bias-variance trade-off can easily be controlled and optimized by changing R, and the number of windows K.

3.3.3 Cohen's Class Interpretation

The MW WVS estimate (3.17) belongs to Cohen's class of time-frequency distributions. We recall this class here as distributions that can be written as

$$C_x(t,f) = W_x(t,f) \;**\; \phi(t,f) \tag{3.18}$$

with $\phi(t,f)$ a kernel function. The kernel generating the spectrogram is precisely the Wigner distribution of the window function. Furthermore, the Wigner distribution of the k-th order Hermite function is the k-th order Laguerre function [21]

$$W_{h_k}(t,f) = L_k(t^2+f^2) = e^{-\frac{\pi}{2}(t^2+f^2)} \sum_{m=0}^{k} \frac{k!}{(k-m)!\,m!} \frac{\left(-\left(\pi\,(t^2+f^2)\right)\right)^m}{m!}. \tag{3.19}$$

Therefore, we have a closed form expression for the kernel corresponding to the MW WVS estimate (3.17) as a weighted sum of K Laguerre functions; in this interpretation, the MW WVS estimate reads

$$\widehat{\mathbf{W}}_x(t,f) = W_x(t,f) \; ** \; \frac{1}{K} \sum_{k=0}^{K-1} L_k(t,f). \tag{3.20}$$

3.3.4 Extraction Of Line Components

As in Thomson's method for stationary signals, the averaging inherent in (3.17) will degrade the resolution of line components. Following Thomson's programme, we will first detect and extract all line components in the data before performing (3.17), and then reshape the estimate. We assume the signal model

$$x(t) = y(t) + \sum_i \mu_i(t)\, e^{j2\pi\gamma_i(t)} \tag{3.21}$$

with $y(t)$ zero mean and Gaussian, and $\mu_i(t)$ the time-dependent amplitude of the line component (Note that $\mu_i(t)$ should not be confused with $\mu(f_i)$ in (3.6) which is the amplitude of the sinusoid at frequency f_i).

A straightforward application of Thomson's sinusoid extraction algorithm to $x(t)$ as in [2, 3] relies on an assumption that the chirp functions $e^{j2\pi\gamma_i(t)}$ can be closely approximated locally as sinusoids. Unfortunately, this is not the case for most chirping components; in these cases, the approach fails. In order to detect and extract highly non-stationary chirps, we have developed a statistical significance test for linear chirps of the form $e^{j2\pi(ft+ct^2)}$. Linear chirps can closely approximate locally all but the most rapidly changing chirp functions.

Algorithm to Detect and Extract Chirp Components

We make the following two basic assumptions:

- Not more than one chirp is present within the circular analysis region of the Hermite window (see Figure 3.4).
- The highest chirping rate c attained by any chirp $e^{j2\pi(ft+ct^2)}$ is $\frac{1}{4T}$, where T is the time support of the analyzing Hermite window.

The chirp detection and extraction algorithm runs as follows:

1. Within the window support T of the window $h(t)$, we approximate the line components as linear chirps

$$\sum_i \mu_i(t)\, e^{j2\pi\gamma_i(t)} \approx \sum_i \mu(f_i, c_i)\, e^{j2\pi(f_i t + c_i t^2)} \tag{3.22}$$

   with $\mu(f_i, c_i)$ the complex amplitude of the linear chirp with offset frequency f_i and chirping rate c_i.

2. We project the data $x(t)$ onto chirps $e^{j2\pi(ft+ct^2)}$ for a fine grid of offset frequencies f, and chirp rates c. This is equivalent to Thomson's F-test (3.10) applied at each frequency and each chirp rate, resulting in a two-dimensional test statistic $F(f, c)$.

3. We repeat the above steps about each time point to obtain the three-dimensional test statistic $F(t, f, c)$.

If the chirping rates of the line components in (3.21) are too high, one needs to use a shorter window in (3.22). However, using a shorter window means that the

line components with lower chirping rates may not be detected, since there may not be enough oscillations of the low frequency sinusoids within the window support T for the F variance-ratio test to detect them. Therefore, for signals containing line components of both high and low chirping rates, it may be necessary to run the above algorithm for different size windows and combine the results in one test statistic.

Spurious Peaks

Due to the repeated application of the test (3.10), the number of spurious peaks in F increases far beyond that seen in Thomson's method for stationary signals (For stationary signals Thomson applies the test for only one chirp rate $c = 0$ since sinusoids are the only stationary deterministic components, whereas we apply it for all time and chirping rates). Roughly speaking, if the test is performed at M chirp rates for each frequency f, then M times more spurious peaks will appear compared to the case when the test is performed at only one chirp rate (that is, $c = 0$). These peaks must be suppressed in order to create a readable time-frequency image.

To suppress spurious peaks that peek above the significance threshold, we employ the following nonlinear cleaning algorithm:

1. Slice $F(t, f, c_j)$ along the chirp-rate dimension.

2. For each c_j, apply a non-linear order statistic filter to $F(t, f, c_j)$ to remove peaks that have not coalesced into a region larger than the Heisenberg uncertainty principle mandates. (Intuition: spurious peaks are isolated in $F(t, f, c_i)$; true peaks lie along curves in $F(t, f, c_i)$.)

3. Combine the results from each c_j to obtain the final test statistic.

Although the linear chirp detection and extraction algorithm is computationally expensive, it is trivially parallelizable.

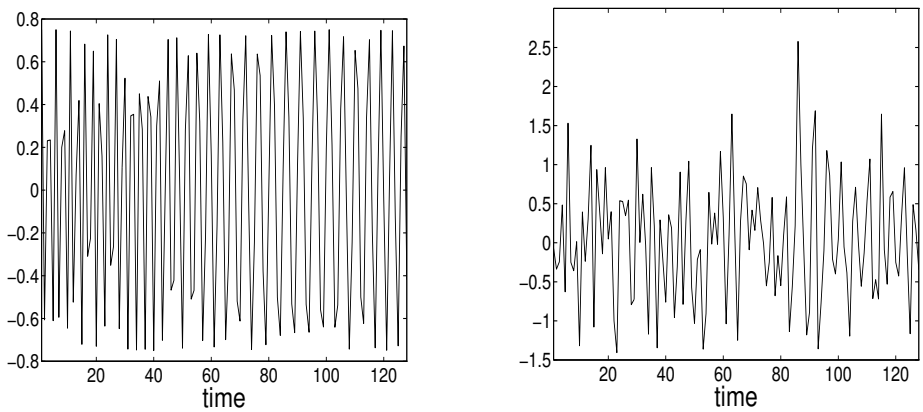

(a) (b)

Figure 3.6: *(a) Test signal composed of a line component of sinusoidal instantaneous frequency. (b) Signal in additive white Gaussian noise 3.23.*

In Figure 3.7, we demonstrate the performance of the linear chirp detection and extraction algorithm, and of the non-linear filtering algorithm using the data shown in Figure 3.6. The data is composed of a line component in additive white Gaussian noise $n(t)$,

$$x(t) = e^{j2\pi(\frac{a}{b}sin(bt)+f_0t)} + n(t) \tag{3.23}$$

with a, b, and f_0 constants. The signal-to-noise ratio is approximately 0.4 dB, and is computed by taking the ratio of the signal power to the noise power. Figure 3.7(a) shows $F(t, f)$ for one chirping rate corresponding to only spurious peaks with no peaks corresponding to "true" line components. They occur as isolated points in the time-frequency plane, and hence can easily be filtered out using a non-linear order statistic filter. Figure 3.7(b) shows $F(t, f)$ for another chirp rate corresponding this time to both spurious peaks, and "true" line components. Clearly, the peaks corresponding to "true" line components form curves, whereas the spurious peaks are still isolated,

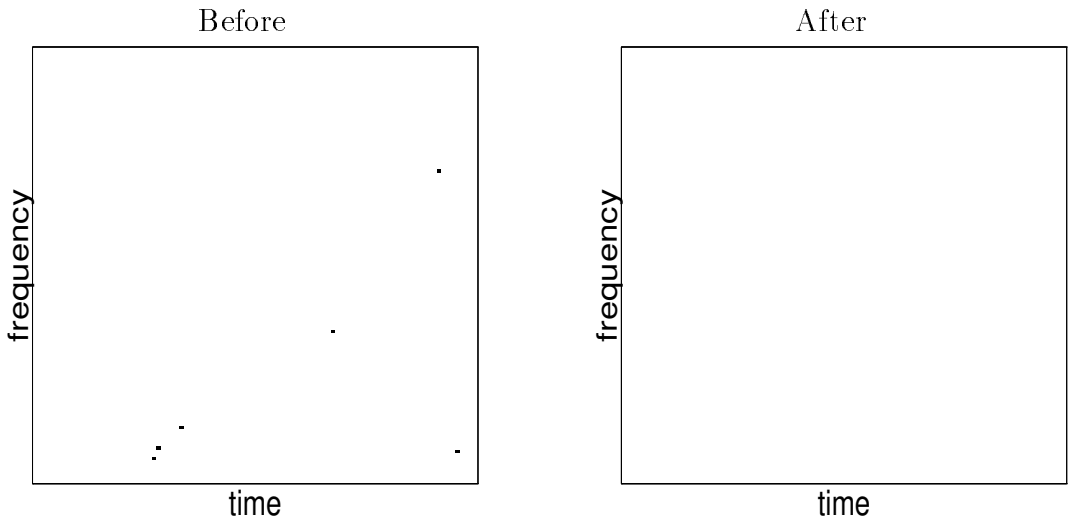

(a)

(b)

Figure 3.7: *Test statistic $F(t, f)$ before and after filtering for two different chirp rates for the test data in 3.23: (a) Corresponding to only spurious peaks. (b) Corresponding to true and spurious peaks.*

and hence can easily be filtered out using the same non-linear order statistic filter as above without affecting the curves.

Impulses and Closely Spaced Chirps

In our line detection and extraction algorithm above, we have not explicitly addressed impulses. Impulses are line components of the form $\delta(t - t_0)$. The Fourier transform of an impulse is the complex sinusoid

$$\delta(t - t_0) \quad \xrightarrow{\text{FT}} \quad e^{j2\pi t_0 f}. \tag{3.24}$$

We can detect and extract impulses from the data by taking the Fourier transform of the data and applying our algorithm on the Fourier transform of the data for chirping rate c equal to zero. Therefore, a different test is not necessary for impulses.

One problem we do not address in this thesis is when several line components cross in the time-frequency plane. The detection algorithm fails about the time-frequency point (t, f) where two or more line components cross. This is due to the fact that the algorithm searches for one line component at a time about each time-frequency point and sees the contribution from the other line components as noise. If N line components co-exist within the analysis region of the window, then it is necessary to search simultaneously for N chirps with parameters (f_i, c_i) for $i = 1, 2, \ldots, N$. This search is extremely expensive, but can be performed if the need arises. In his paper [15], Thomson discusses simultaneous searches for N closely spaced sinusoids, and gives an algorithm for the case when $N = 2$. Of course, the performance of the F-test declines as the number of sinusoids within the analysis region of the window increases. Nonetheless this algorithm can be modified to search for two linear chirps that co-exist in the analysis region of the window.

Other Line Detection Algorithms

Although we do not use them in this thesis, we would still like to mention two other line component detection algorithms. They are the reassignment method and the "snakes" method.

The reassignment method is a scheme to increase the readability of the existing TFRs. It was first introduced in 1976 by Kodera, Gendrin and Villedary [22, 23] for the spectrogram. Auger and Flandrin extended the method to the general time-frequency and time-scale representations [24]. Here, we will briefly explain how the method works for the distributions in Cohen's class.

When we look at the distributions in Cohen's class

$$C_x(t,f) = \int\int \phi(u,v)\, W_x(u-t, v-f)\, dudv \tag{3.25}$$

we see that the value of C_x at the time-frequency point (t,f) is the sum of all the terms $\Phi(t,f)\, W_x(t-u, f-v)$. These terms can be considered as contributions of the weighted Wigner distributions from the neighboring points, delimited essentially by the support of the kernel $\Phi(t,f)$. As Figure 3.8 shows C_x can be non-zero at a point (t,f) even when the WD indicates no energy. What the reassignment method does is to assign the value computed at (t,f) to the center of gravity (t',f') of the energy distributions $\Phi(t,f)\, W_x(t-u, f-v)$.

The assignment method can be used as a line detection algorithm because it performs perfect localization of chirps and impulses. Of course, the performance of the method degrades in the presence of noise. Chassande-Mottin, Auger, and Flandrin address the reassignment method in the presence of noise in their paper [25].

Although the "snakes" method is not the kind of line detection we are interested in, we would like to give the main idea behind it. The method due to Carmona, Hwang and Torrèsani, detects lines in the data by looking at the ridges of their wavelet transforms [26].

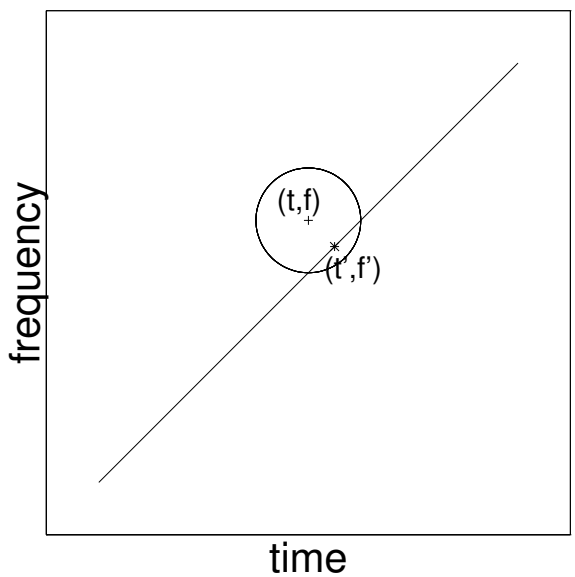

Figure 3.8: *Reassignment method: The value of the TFR computed at point* (t, f) *is assigned to the point* (t', f').

3.4 Multiple Window Time-Scale Analysis

For random processes containing high frequency components of short duration and low frequency components of long duration, time-frequency techniques are not appropriate. These types of processes are better matched by time-scale representations from the affine class [12]. The smoothing kernels in the affine class change with frequency to accommodate high frequency components of short duration and low frequency components of long duration. The regions of smoothing at different parts in

the time-frequency plane for Cohen's class and the affine class are shown in Figure 3.9.

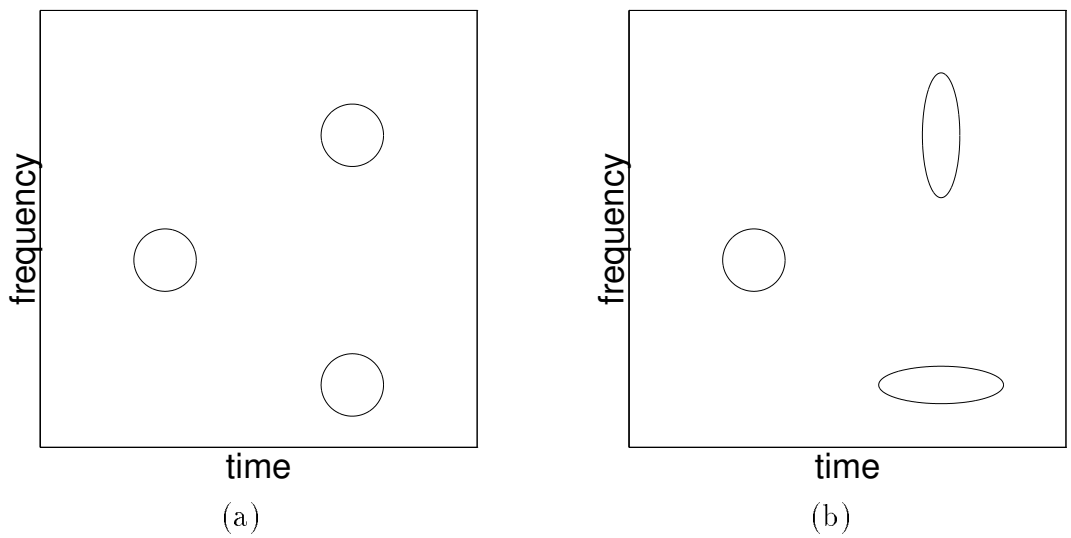

Figure 3.9: *Smoothing regions in the time-frequency plane in (a) Cohen's class, (b) Affine class.*

3.4.1 Morse Wavelets

The Morse wavelets [7,27,28] play a rôle in time-scale analogous to that of the Hermite windows in time-frequency. The k-th order Morse wavelet[3] is defined in the frequency domain as

$$\Psi_k(f) = f^{\beta/2}\, e^{-f^\gamma/2}\, \frac{d^\beta}{df^\beta}\left[e^{f^\gamma}\, \frac{d^{\beta+k}}{df^{\beta+k}}\left(f^{\beta+k}\, e^{-f^\gamma}\right)\right], \tag{3.26}$$

with $k = 0, 1, 2, \cdots$, $\beta > 0$ the degree of flatness at $f = 0$, and $\gamma > 0$. The Morse wavelets are the eigenfunctions of a localization operator over a tear-drop shaped region whose exact shape depends on β and γ [28]. For the special case $\beta = \gamma = 1$,

[3]In fact, Morse defined a special case of these wavelets for $\gamma = 0$ in [27], but we still call the general class that is due to Daubechies and Paul [28] the Morse wavelets.

the Morse functions are mutually orthogonal and maximally concentrated in the time-frequency region which can be written as [7, 28]

$$\left\{(t,f): \quad t^2 + \frac{9}{4f^2} + 1 \leq \frac{3C}{|f|}\right\} \tag{3.27}$$

with C a constant.[4]. We show this region in Figure 3.10(a). For β and γ equal one, the eigenvalues of the bandpass localization operator corresponding to the Morse wavelets are given by

$$\lambda_k(C) = (k+1)\left(\frac{C-1}{C+1}\right)^{k+1}\left(\frac{2}{C+1}\,\frac{1}{k+1}\right). \tag{3.28}$$

There is no closed form expression for the eigenvalues for any other choices of β and γ. We show the behavior of the eigenvalues in Figure 3.10(b). We can see that for a given C, only a certain number of the eigenvalues are close to one, therefore only the first few Morse wavelets corresponding to those eigenvalues have excellent concentration.

Figure 3.11 shows the first three Morse wavelets in time, their Fourier transforms, and their Wigner distributions. Comparing this figure with Figure 3.10(a), one can see how the shape of the Wigner distribution of each Morse wavelet matches the shape of the concentration region.

3.4.2 Multiple Window WVS Estimate

We form a time-scale MW WVS estimate of the data $x(t)$ as the weighted average of the squares of K wavelet transforms using the Morse wavelets

$$\widehat{\mathbf{W}}_x(t,a) \;=\; \frac{1}{K}\sum_{k=0}^{K-1}\left| a^{-1/2}\int x(\tau)\,\psi_k\!\left(\frac{\tau-t}{a}\right)d\tau\right|^2. \tag{3.29}$$

[4]The formula for the concentration region for any β and γ can be found in [28].

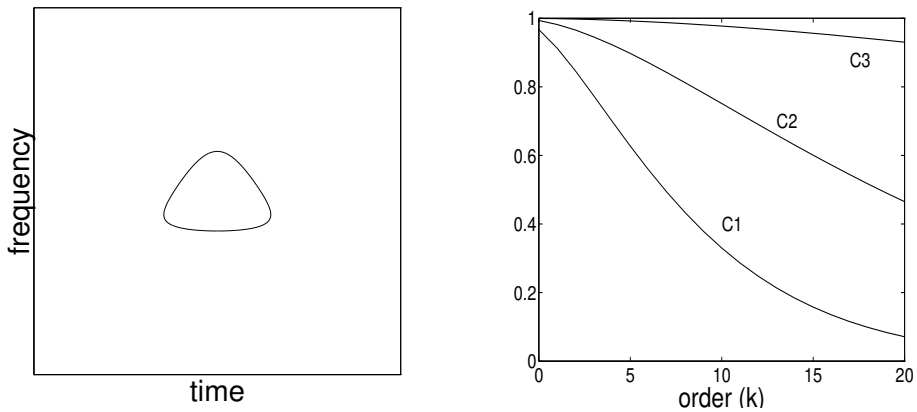

(a) (b)

Figure 3.10: *(a) The tear-drop shaped concentration region (3.27) for the Morse wavelets for $\beta = \gamma = 1$ equal to. (b) Eigenvalues of the localization operator for different values of C ($C_1 < C_2 < C_3$) for $\beta = \gamma = 1$.*

where ψ_k is the k-th order Morse wavelet expressed in the time domain. The value of K depends on the choice of C in the concentration region. For low bias we need small C, but for low variance a large C is needed so that more eigenvalues are close to one. Therefore, we again see the bias-variance trade-off. The resulting estimate belongs to the affine class of time-scale covariant distributions. Its kernel is the weighted sum of the Wigner distributions of the K Morse wavelets.

As in the time-frequency case, averaging degrades the resolution of chirping line components. Using the algorithm of Section 3.3.4, we can detect and extract the line components from the data before computing the estimate (3.29).

Lilly and Park have also considered multi-wavelet spectrum estimation [29]. In their work, they employed different wavelets and did not consider line component extraction.

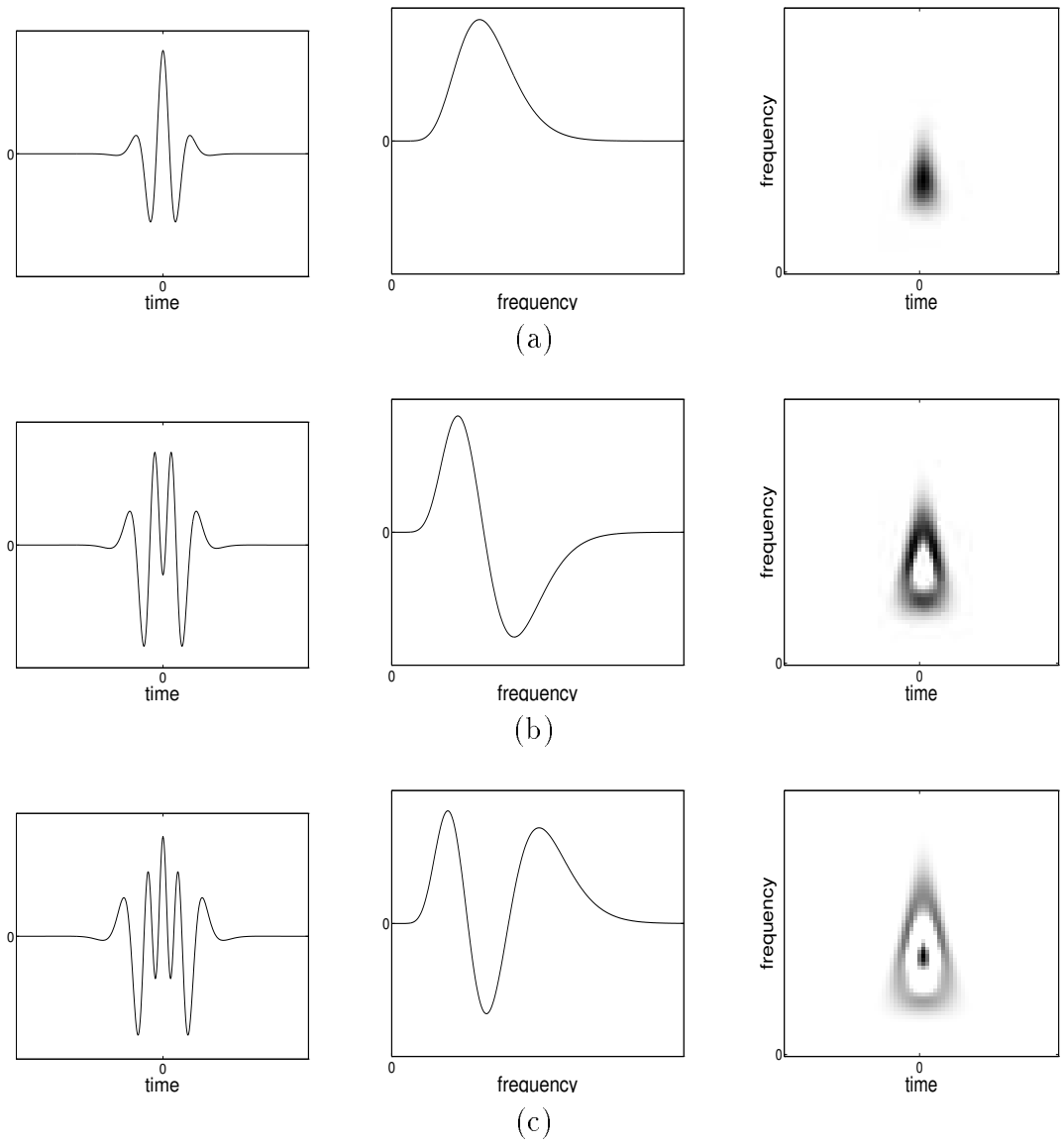

Figure 3.11: *From left to right the first three Morse wavelets in the time domain, the frequency domain (only the positive frequencies), and the time-frequency plane (WD): (a) 0-th order, (b) 1-st order, (c) 2-nd order.*

3.5 Examples

For our first example we refer to Figure 3.1. In this figure we illustrate the performance of the MW WVS estimate using a test signal composed of a chirp with sinusoidal instantaneous frequency in an additive bandpass Gaussian noise of linearly rising center frequency. The signal in time domain and its ideal representation in time-frequency is shown in 3.1(a) and 3.1(b). It is not possible to identify the components of the test signal from the empirical Wigner distribution due to its large variance. The spectrogram smoothes the Wigner distribution. Unfortunately the amount of smoothing needed to reduce the variance smears the line components excessively. A sliding version of Thomson's method as proposed in [1–3] does not perform well for this non-stationary data, since a local sine approximation to the chirping line component is inadequate. The time-frequency MW estimate of Figure 3.1(f) on the other hand has both high resolution and low variance simultaneously. The computed variance of the MW WVS estimate is approximately $\frac{1}{4}$ that of the spectrogram, which agrees with the fact that four windows were used in the computation of the MW WVS estimate.

In Figure 3.12, we demonstrate the ability of the linear chirp detection algorithm to detect four hyperbolic chirps simultaneously. The data is a digitized 2.5 microsecond echo-location pulse emitted by the Large Brown Bat, Eptesicus Fuscus. There are 400 samples and the sampling period is 7 microseconds. Comparing the multiple window method with the other two plots, we see that the detection algorithm is able to pull out even the weakest high frequency line component successfully. The method even reveals the aliasing of the hyperbolic chirp due to under-sampling.

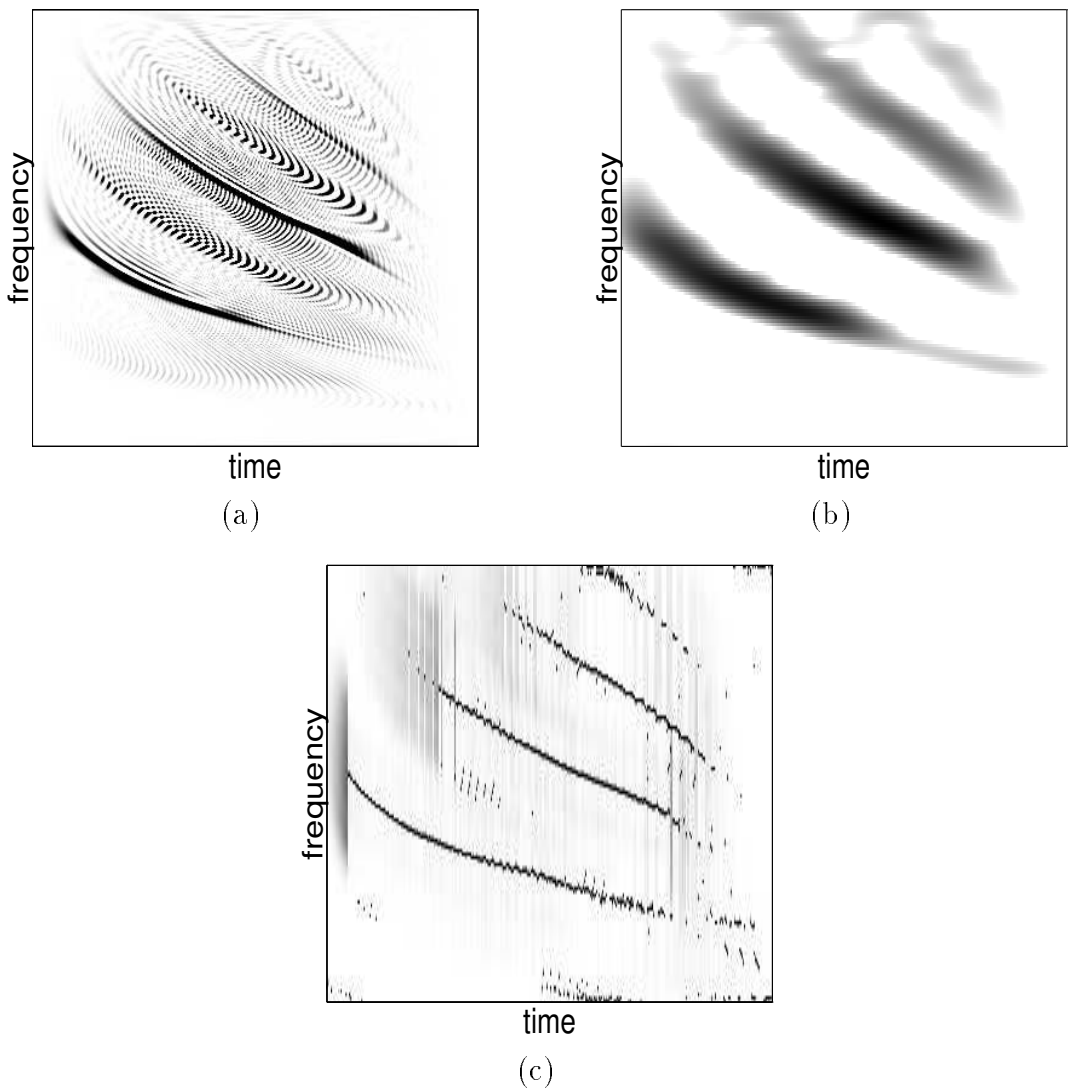

Figure 3.12: *Three spectrum estimates of the echo-location pulse emitted by the Large Brown Bat, Eptesicus Fuscus: (a) Empirical Wigner distribution. (b) Spectrogram. (c) Multiple window method.*

Chapter 4

Discussion and Conclusions

In this thesis, we have motivated and developed multiple-window time-frequency and time-scale analysis for time-varying signals by extending Thomson's work [15] on multiple-window spectrum estimation for stationary signals.

Our contribution differs from the previous work done in multiple-window method spectrum estimation of time-varying signals in two major ways:

1. We have identified the optimal windows to use for time-varying spectrum estimation. They are the Hermite functions [18–20] for time-frequency analysis, and the Morse wavelets [7, 27, 28] for time-scale analysis. These windows are optimal in the sense that they are the most concentrated set of orthogonal functions in the time-frequency and time-scale planes resulting in low bias spectral estimates.

2. We have developed an algorithm to detect and extract non-stationary line components from the data by approximating them as piece-wise linear chirps. We then form the MW WVS estimate of the chirp-free data and reshape the spectrum to account for the excised line components. This preserves the resolution of the line components.

The line detection and extraction algorithm is computationally expensive, especially if one needs to run the algorithm for different window sizes as suggested in

Section 3.3.4. This problem can be overcome using parallel processors since the nature of the algorithm makes it readily parallelizable.

Bibliography

[1] G. Frazer and B. Boashash, "Multiple window spectrogram and time-frequency distributions," in *Proc. IEEE Int. Conf. Acoust., Speech, Signal Processing — ICASSP '94*, vol. IV, pp. 293–296, 1994.

[2] K. A. Farry, *Issues in Myoelectric Teleoperation of Complex Artificial Hands.* Ph.D. dissertation, Dep. Elec. Comput. Eng., Rice University, 1994.

[3] K. A. Farry, R. G. Baraniuk, and I. D. Walker, "Nonparametric, low bias, and low variance time-frequency analysis of myoelectric signals," in *International Conference of the IEEE Engineering in Medicine and Biology Society (EMBS), Montreal, Canada*, Sept. 1995.

[4] S. M. Kay, *Modern Spectral Estimation.* Prentice Hall, 1988.

[5] L. Cohen, *Time-Frequency Analysis.* Englewood Cliffs, NJ: Prentice-Hall, 1995.

[6] M. B. Priestley, *Non-Linear And Non-Sationary Time Series Analysis.* Academic Press, 1988.

[7] I. Daubechies, *Ten Lectures on Wavelets.* New York: SIAM, 1992.

[8] L. Cohen, "Time-frequency distributions — A review," *Proc. IEEE*, vol. 77, pp. 941–981, July 1989.

[9] W. Martin and P. Flandrin, "Wigner-Ville spectral analysis of nonstationary random processes," *IEEE Trans. Acoust., Speech, Signal Processing*, vol. 33, pp. 1461–1470, Dec. 1985.

[10] O. Rioul and M. Vetterli, "Wavelets and signal processing," *IEEE Signal Processing Mag.*, vol. 8, pp. 14–38, Oct. 1991.

[11] F. Hlawatsch and G. F. Boudreaux-Bartels, "Linear and quadratic time-frequency representations," *IEEE Signal Processing Mag.*, vol. 9, pp. 21–67, Apr. 1992.

[12] O. Rioul and P. Flandrin, "Time-scale energy distributions: A general class extending wavelet transforms," *IEEE Trans. Signal Processing*, vol. 40, pp. 1746–1757, July 1992.

[13] H. I. Choi and W. J. Williams, "Improved time-frequency representation of multicomponent signals using exponential kernels," *IEEE Trans. Acoust., Speech, Signal Processing*, vol. 37, pp. 862–871, June 1989.

[14] A. M. Sayeed and D. L. Jones, "Optimal kernels for nonstationary spectral estimation," *IEEE Trans. Signal Processing*, vol. 43, pp. 478–491, Feb. 1995.

[15] D. J. Thomson, "Spectrum estimation and harmonic analysis," *Proc. IEEE*, vol. 70, pp. 1055–1096, Sept. 1982.

[16] D. J. Thomson. Personal Communication.

[17] D. Slepian and H. O. Pollack, "Prolate spheroidal wave functions, Fourier analysis and uncertainty," *Bell Syst. Tech. J.*, vol. 40, pp. 43–64, Jan. 1961.

[18] I. Daubechies, "Time-frequency localization operators: A geometric phase space approach," *IEEE Trans. Inform. Theory*, vol. 34, pp. 605–612, July 1988.

[19] P. Flandrin, "Maximum signal energy concentration in a time-frequency domain," in *Proc. IEEE Int. Conf. Acoust., Speech, Signal Processing — ICASSP '88*, pp. 2176–2179, 1988.

[20] T. W. Parks and R. G. Shenoy, "Time-frequency concentrated basis functions," in *Proc. IEEE Int. Conf. Acoust., Speech, Signal Processing — ICASSP '90*, vol. 5, pp. 2459–2462, 1990.

[21] G. B. Folland, *Harmonic Analysis in Phase Space.* Princeton, NJ: Princeton University Press, 1989.

[22] K. Kodera, C. D. Villedary, and R. Gendrin, "A new method for the numerical analysis of non-stationary signals," *Phys. Earth and Plan. Int.*, vol. 12, pp. 142–150, 1976.

[23] K. Kodera, R. Gendrin, and C. D. Villedary, "Analysis of time-varying signals with small bt values," *IEEE Trans. Acoust., Speech, Signal Processing*, vol. ASSP-26, no. 1, pp. 64–76, 1978.

[24] F. Auger and P. Flandrin, "Improving the readability of time-frequency and time-scale representations by the reassignment method," *IEEE Trans. Signal Processing*, vol. 43, pp. 1068–1089, May 1995.

[25] E. Chassande-Mottin, F. Auger, and P. Flandrin, "Supervised time-frequency reassignment," in *IEEE SP International Symposium on Time-Frequency and Time-Scale Analysis*, June 1996.

[26] R. A. Carmona, W. L. Hwang, and B. Torrèsani, "Characterization of signals by the ridges of their wavelet transforms." Mar. 1995.

[27] P. Morse, "Diatomic molecules according to the wave mechanics II. Vibrational levels," *Physical Review*, vol. 34, pp. 57–64, July 1929.

[28] I. Daubechies and T. Paul, "Time-frequency localization operators — a geometric phase space approach: II. The use of dilations," *Inverse Problems*, no. 4, pp. 661–680, 1988.

[29] J. M. Lilly and J. Park, "Multiwavelet spectral and polarization analyses of seismic records," *Geophys. J. Int.*, no. 122, pp. 1001–1021, 1995.